Editors' Suggestion | Featured in Physics

Surface Triple Junctions Govern the Strength of a Nanoscale Solid

Ye-Yuan Zhang,[1,2] Hui Xie,[1] Ling-Zhi Liu,[1] and Hai-Jun Jin[1,*]

[1]*Shenyang National Laboratory for Materials Science, Institute of Metal Research, Chinese Academy of Sciences, Shenyang 110016, People's Republic of China*

[2]*School of Materials Science and Engineering, University of Science and Technology of China, Shenyang 110016, People's Republic of China*

(Received 28 January 2021; revised 11 April 2021; accepted 10 May 2021; published 11 June 2021)

Surface triple junctions (STJs), i.e., the termination lines of grain boundaries at solid surface, are the common line defects in polycrystalline materials. Compared with planar defects such as grain boundaries and surfaces, STJ lines are usually overlooked in a material's strengthening although abundant atoms may reside at STJs in many nanomaterials. In this study, by *in situ* compression of coarse-grained and nanocrystalline nanoporous gold samples in an electrochemical environment, the effect of STJs on the strength of nanoporous gold was successfully decoupled from *grain-boundary* and *surface effects*. We found that the strength of nanoporous gold became sensitive to STJ modification when ligament size was decreased to below ~100 nm, indicating that STJs started to influence ligament strength at sub-100 nm scale. This *STJ effect* was associated with the emission of dislocations from STJs during plastic deformation. Our findings strongly suggest that the structure and chemistry at STJs should be considered in understanding the mechanical response of sub-100 nm scale materials.

DOI: 10.1103/PhysRevLett.126.235501

Nanoscale materials are widely used in modern technologies such as microelectronics, batteries, chemical, and electrochemical devices. Many nanomaterials (e.g., thin films, nanowires, nanoporous materials) are polycrystals with a large fraction of atoms residing at surfaces, grain boundaries, and the termination lines of grain boundaries at surface [i.e., surface triple junctions (STJs)] [1]. The strength of these materials, which is critical to many applications, has been extensively studied with focus on sample-size and grain-size effects, in other words, the effects of surfaces and grain boundaries on plastic deformation [2–5]. However, the effects of STJs and STJ modifications on strength were largely overlooked previously, although dislocation nucleations at STJs have been reported in some previous studies [5,6]. STJs were often linked to grain growth [7–9], surface roughening [8,10], and catalysis [11], but not the material strength. The *STJ effect* may (or may not) have contributed to the hardness measured on individual STJs [12], and the strengths of polycrystalline thin films [2] or other nanoscale solids [3–5] containing high-density STJs. But it is extremely difficult to decouple the STJ effect, if there is any, from *grain-boundary* and *surface effects*. The main challenge comes from the fact that the quantities of STJs and abutting planar defects (grain boundaries and surfaces) do not vary independently.

In this study, we decoupled STJ effect from surface and grain-boundary effects by *in situ* compression of nanoporous gold (NPG) in an electrochemical environment. Each NPG is a macroscopic assembly of a huge number of gold nanoligaments. For example, in NPG with ligament size of 100 nm, there are $\sim 10^{12}$ ligaments in a 1 mm^3 cubic sample. The strength of such a sample then reflects the mean strength of 10^{12} nanoligaments with controlled defects, as expressed by Gibson-Ashby scaling laws [13]. On one hand, surface effect can be separated from the combined STJ and grain-boundary effects by comparing the mechanical responses of two types of NPGs: nanocrystalline NPG (NC-NPG) containing large quantities of surfaces, grain boundaries, and STJs, and coarse-grained NPG (CG-NPG) with large surface area but very few grain boundaries and STJs. On the other hand, the grain-boundary effect can be separated from the combined surface and STJ effects by monitoring the variation of material's strength in response to electrochemical modifications, because grain boundaries buried in gold ligaments are inert to electrochemistry. With these approaches combined, we uncovered that STJ effect became pronounced in NPGs with ligament size below ~100 nm. This critical size is 2 orders of magnitude larger than the previous prediction of ~3 nm, below which the fraction of atoms at triple junctions exceeds that at grain boundaries in nanocrystalline solids [14].

NC-NPG was fabricated by dealloying [15,16] or selectively dissolving Al from an Al_2Au compound (see Supplemental Material [17]). Transmission electron microscopy [(TEM), see Fig. 1(a)] and a precession electron diffraction (PED) orientation map [Fig. 1(b)] show that grain size is on the same order of ligament diameter in this material. As a reference sample, CG-NPG dealloyed

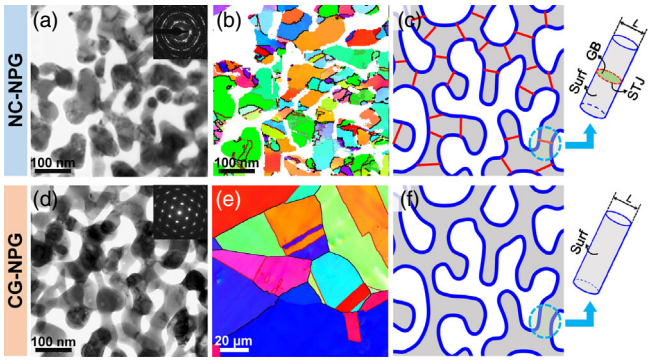

FIG. 1. NPG with high-population STJs. (a) TEM image and an inset selected area electron diffraction (SAED) pattern, (b) PED orientation map, and (c) a schematic illustration of NC-NPG structure. (d) TEM image and an inset SAED pattern, (e) EBSD orientation map, and (f) a schematic illustration of the structure of CG-NPG. Grain boundary (GB).

from $Ag_{75}Au_{25}$ [18] exhibits similar morphology and ligament size [~45 nm; see Fig. 1(d)], but several orders of magnitude larger grain sizes [10^2–10^3 μm, Fig. 1(e)] compared with NC-NPG. NP structure can be coarsened by annealing, during which the large grain size of CG-NPG was conserved (Fig. S1 [17]), while the grain size and ligament size remained equivalent for NC-NPG (Figs. S2–S3 [17]). Most grain boundaries intersect with surfaces, forming high-population STJs in NC-NPG. As illustrated in Figs. 1(c) and 1(f), grain boundaries and STJs are few in CG-NPG, but abundant in NC-NPG, while both NPGs exhibit large surface area. For clarity, in this Letter, STJ is not considered as a part of a surface, and the surface refers to a STJ-free surface if not mentioned otherwise.

Millimeter-sized NPG was compressed *in situ* while all pores were infiltrated with electrolytes [see Fig. 2(a)] and the surface (including STJs) was modified by applying a potential [18]. This allows for quantifying the effect of electrochemical modification on NPG's strength while the characteristic size and geometry structure remain unchanged. Figure 2(b) shows that the shape of cyclic voltammogram (CV) curves of NC- and CG-NPGs are very similar, indicating the surface structure and surface electrochemical processes are almost identical in both NPGs (see also Fig. S4 [17]). Furthermore, anodic peaks corresponding to {111} and {001} facets [26] were not evident in CVs shown in Fig. 2(b), indicating that surface faceting is not severe for both NC- and CG-NPGs. This study focused on two states: at 1.53 V, the Au surface was covered with oxygen adsorbate or monolayer oxide [27]; at 1.13 V, monolayer oxide was lifted to obtain a relatively clean surface. The STJ state is identical to the surface state throughout this Letter. In the following, CLN and ORD stand for the clean and oxidized states, respectively.

For both CG-NPG [Fig. 2(c)] and NC-NPG [Fig. 2(d)], at a compression strain of 0.10, flow stresses increased abruptly as applied potential increased from 1.13 to 1.53 V, while the surface changed from clean to the oxidized state. This agrees with previous reports on CG-NPG [18,28,29]

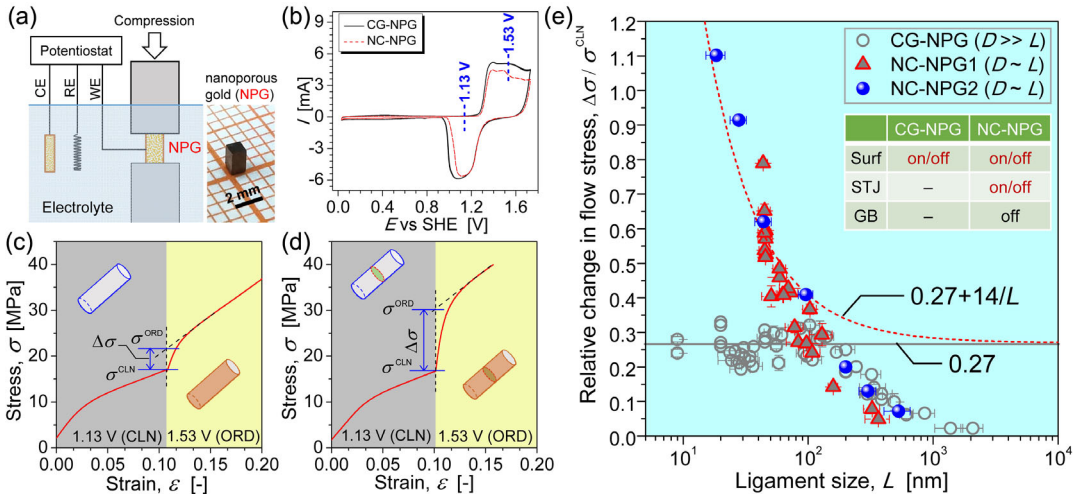

FIG. 2. *In situ* compression of NPG in an electrochemical environment. (a) Schematic illustration of an electrochemical cell for *in situ* compression. Working electrode (WE). Reference electrode (RE). Counter electrode (CE). (b) Cyclic voltammogram of CG-NPG and NC-NPG in 1 M $HClO_4$ at 5 mV/s. Compressive engineering stress-strain curves of (c) a typical CG-NPG ($L = 32$ nm) and (d) a typical NC-NPG ($L = 43$ nm) measured *in situ* under electrochemical control, with potential jumping from 1.13 to 1.53 V at a strain of approximately 0.10. The strain rate is 10^{-4} s^{-1}. (e) Monolayer oxide induced increase in flow stress, $\Delta\sigma/\sigma^{CLN}$, plotted as a function of ligament size L, for CG-NPG, NC-NPG1 dealloyed from Al_2Au, and NC-NPG2 obtained by compressing CG-NPG to a strain of 0.55 (see more details in Figs. S3 and S5 [17]). Grain size (D). Some data of CG-NPG are adapted from Refs. [18,28]. Inset table shows major defects and their sensitivity to electrochemical modifications (on/off: sensitive; off: insensitive; –: this defect is very few or does not exist).

and the surfactant-induced strengthening recently reported in other nanoscale single crystals [30,31].

The strength or flow stress of a porous material σ is proportional to the strength of its solid ligaments σ_{lig}, by $\sigma = f(\varphi, g)\sigma_{\mathrm{lig}}$, where $f(\varphi, g)$ is a scaling parameter controlled by relative density φ and topology parameter such as the scaled genus density g [19,32–34]. At the point of potential jumping, when the surface was switched from a clean to oxidized state, the geometrical structure of NPG and thus $f(\varphi, g)$ remained unchanged. Then, $f(\varphi, g)$ is canceled out in the expression of relative change in flow stress:

$$\Delta\sigma/\sigma^{\mathrm{CLN}} = \Delta\sigma_{\mathrm{lig}}/\sigma_{\mathrm{lig}}^{\mathrm{CLN}}, \tag{1}$$

where the superscripts CLN and ORD represent clean (at 1.13 V) and oxidized (at 1.53 V) surface states, respectively. Here, $\Delta\sigma = \sigma^{\mathrm{ORD}} - \sigma^{\mathrm{CLN}}$ and $\Delta\sigma_{\mathrm{lig}} = \sigma_{\mathrm{lig}}^{\mathrm{ORD}} - \sigma_{\mathrm{lig}}^{\mathrm{CLN}}$ are oxidation-induced net changes in the flow stress of NPG [see Figs. 2(c)–2(d)] and nanoligaments, respectively. Within the scope of this study, $\Delta\sigma/\sigma^{\mathrm{CLN}}$ is insensitive to NPG's aspect ratio (Fig. S6 [17]), relative density (Fig. S7 [17]), and topology structure, and reflects the proportional increase of the ligament's strength ($\Delta\sigma_{\mathrm{lig}}/\sigma_{\mathrm{lig}}^{\mathrm{CLN}}$) induced by monolayer-oxide coverage.

As summarized in Fig. 2(e), for CG-NPG, $\Delta\sigma/\sigma^{\mathrm{CLN}}$ increases from near zero to 0.27 when ligament diameter L decreases from few μm to approximately 100 nm, then saturates at 0.27 as L decreases further. The $\Delta\sigma/\sigma^{\mathrm{CLN}}$ values of NC-NPG coincide with that of similar ligament-sized CG-NPG for $L > 100$ nm, but significantly deviate from and exceed that of CG-NPG at $L < 100$ nm. For NC-NPG, $\Delta\sigma/\sigma^{\mathrm{CLN}}$ increases monotonically (to 1.10 at $L = 18$ nm) with decreasing L and does not saturate in the tested size range.

NC-NPGs were prepared by two different routes: NC-NPG1 was dealloyed from Al_2Au; NC-NPG2 was obtained by compressing CG-NPG to a large strain of 0.55, where the grain size was refined to the same scale of ligament size (see Fig. S3 [17]). As shown in Fig. 2(e), the data of NC-NPG1 and NC-NPG2 are consistent with each other. This rules out residual Al (<2 at.%) in NC-NPG1, pre-existing dislocations in NC-NPG2, and other difference in structural features (such as surface tortuosity) arising from different precursor alloys and synthesis methods, as the major cause of their large $\Delta\sigma/\sigma^{\mathrm{CLN}}$ values displayed in Fig. 2(e).

The size-insensitive $\Delta\sigma/\sigma^{\mathrm{CLN}}$ observed in CG-NPG with $L < \sim$100 nm can be attributed to a surface-controlled deformation mode (surface dislocation nucleation) in Au nanoligaments [28], which has been widely observed in sub-100 nm FCC single crystals [35–37]. For ~100 nm $< L <$ ~1 μm, the decrease of $\Delta\sigma/\sigma^{\mathrm{CLN}}$ with increasing L is associated with the increasing contribution of "bulklike" collective dislocation dynamics (dislocation interactions and multiplications) in larger ligaments. Such bulklike plasticity is insensitive to surface modifications, and thus reduces $\Delta\sigma/\sigma^{\mathrm{CLN}}$ if it contributes more to deformation. Eventually, surface effect vanishes while bulklike behavior becomes dominant, and in consequence, $\Delta\sigma/\sigma^{\mathrm{CLN}}$ diminishes to near zero as L increases to the μm scale.

Unlike CG-NPG, NC-NPG contains high-density grain boundaries and STJs. Because grain boundaries are buried within the bulk, grain-boundary-mediated plasticity (e.g., dislocation nucleation from grain boundaries or other grain-boundary dislocation interactions) is insensitive to electrochemical modifications, similar to the bulklike deformation involved in the deformation of CG-NPG with $L > 100$ nm. The grain-boundary dominated plasticity would decrease $\Delta\sigma/\sigma^{\mathrm{CLN}}$, which contradicts the larger $\Delta\sigma/\sigma^{\mathrm{CLN}}$ values observed in NC-NPG with $L < 100$ nm (compared with CG-NPG). The deformation of NC-NPG is unlikely controlled by grain-boundary-mediated processes.

The only defect that is abundant in NC-NPG but few in CG-NPG, and can be electrochemically modified (see inset table in Fig. 2(e)) is STJ, which might account for the large $\Delta\sigma/\sigma^{\mathrm{CLN}}$ of NC-NPG with $L < 100$ nm. It is reasonable to assume that the plastic deformation of NPG with $L < 100$ nm is controlled by dislocation nucleations at surface or STJs. The stresses for dislocation nucleation σ_{nucl} increases by $\Delta\sigma_{\mathrm{nucl}}$ (net change) or $\delta = \Delta\sigma_{\mathrm{nucl}}/\sigma_{\mathrm{nucl}}$ (relative change) after monolayer oxidation. For dislocation nucleation at surfaces and STJs, δ values are δ_{Surf} and δ_{STJ}, respectively. In CG-NPG with $L < 100$ nm, dislocations mostly nucleate from the surface (Surf); thus $\delta_{\mathrm{Surf}} = \Delta\sigma/\sigma^{\mathrm{CLN}}$ or $\delta_{\mathrm{Surf}} = 27\%$. In NC-NPG with $L < 100$ nm, for simplicity, we assume that the probabilities of dislocation nucleations at surface and STJs are proportional to their fractions of atoms and insensitive to surface state. An alternative to this assumption is that the mean strength of ligaments in NC-NPG is a weighted average value of the strengths of STJ-free and STJ-dominated ligament segments. Then we obtain

$$\Delta\sigma/\sigma^{\mathrm{CLN}} = \delta_{\mathrm{Surf}} + (\delta_{\mathrm{STJ}} - \delta_{\mathrm{Surf}})\xi/L. \tag{2}$$

Here, ξ is the width and ξ/L ($0 < \xi/L < 1$) is the fraction of STJ-affected region on total surface (including STJs), on assumption of equivalent grain and ligament sizes. As shown in Fig. 2(e), the data of NC-NPG ($L < 100$ nm) can be fitted very well using this expression—note that this analysis does not consider bulklike plasticity that is responsible for the diminishing $\Delta\sigma/\sigma^{\mathrm{CLN}}$ at $L > 100$ nm for both type of NPGs. In this scenario, $\Delta\sigma/\sigma^{\mathrm{CLN}}$ of NC-NPG would saturate at δ_{STJ} when L becomes smaller than ξ, where the deformation is fully controlled by STJ-initiated dislocation nucleations. The fitting of NC-NPG data gives $\xi(\delta_{\mathrm{STJ}} - 0.27) = 14$ nm, hinting that $\Delta\sigma/\sigma^{\mathrm{CLN}}$ may saturate at sub-10 nm scale (depending on δ_{STJ} value).

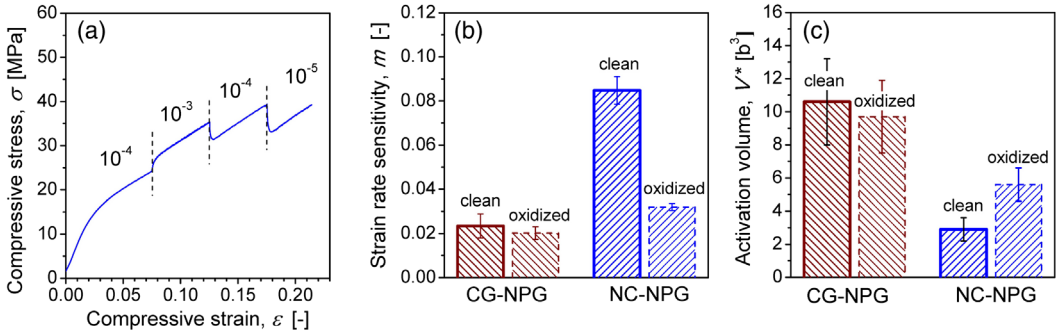

FIG. 3. Strain-rate sensitivity and activation volume. (a) Typical engineering stress-strain curves of NPG under compression obtained by strain-rate jump tests (NC-NPG with clean surface). (b) Strain-rate sensitivity m and (c) activation volume for CG- and NC-NPG samples with similar ligament sizes (~45 nm) but different surface states.

The deformation kinetics is also different in CG- and NC-NPGs, as shown in Fig. 3. Strain-rate jump tests [Fig. 3(a)] were conducted to measure strain-rate sensitivity, $m = d\ln(\sigma)/d\ln(\dot{\varepsilon})$, where σ and $\dot{\varepsilon}$ are the flow stress of NPG and strain rate, respectively. The activation volume [36] for deformation is then derived as $V^* = \sqrt{3}k_BT/(\sigma_{\rm lig}m)$, where k_B is the Boltzmann constant, T the absolute temperature, and $\sigma_{\rm lig}$ the corrected strength (Fig. S8 [17]) of nanoligaments [19].

As shown in Figs. 3(b)–3(c), for CG-NPG ($L = 45$ nm) with a clean surface, $m = 0.02$ and $V^* = 10.6 \pm 2.6\ b^3$, where b is the magnitude of the full FCC Burgers vector. This V^* value agrees well with the data ($10\ b^3$) reported for dislocation nucleation at atomically smooth surfaces [36]. Both parameters (m, V^*) of CG-NPG change little after oxidation, implying that the kinetics of surface dislocation nucleation is insensitive to electrochemical modification.

For NC-NPG (with $L = 45$ nm), m (~0.08) is larger and V^* ($2.9 \pm 0.7\ b^3$) is smaller than those of CG-NPG. Furthermore, m decreases to 0.03 and V^* increases to $5.6 \pm 1.0\ b^3$ after oxidation. This confirms again the essential roles of STJs played in NC-NPG deformation, because m and V^* are insensitive to monolayer oxidation for both surface-mediated (as in CG-NPG) and grain-boundary-mediated deformation.

The increase of V^* of NC-NPG after monolayer oxidation implies that either (i) the V^* for dislocation nucleation at STJs has increased, similar to that at the corners of gold nanowires after thick-oxide coating [38], or (ii) V^* values for dislocation nucleation at each site remained unchanged but the fraction of dislocation-nucleation events at STJ-free surfaces (with larger V^*) has increased. The two mechanisms may be distinguished in the future by examining NC-NPG with sufficiently small L, where the deformation is fully controlled by dislocation nucleation at STJs. Such experiment would uncover the width of the STJ-affected region (ξ value), and clarify whether the dislocation nucleation at STJs is a diffusion-mediated process similar to that observed at corner sites ($V^* = 0.13\ b^3$) of Pd nanowires [39,40], and eventually whether the material is weakened by STJs at nanometer scale (see Fig. S8 [17]).

The traces of dislocation nucleations were indeed observed in compressed NC-NPG, as shown in Fig. 4. These are stacking faults generated by the nucleation and passing of leading partial dislocations. Most likely, Figs. 4(a)–4(b) show the traces of dislocation nucleation at STJs rather than at grain boundaries. As discussed earlier, if the deformation of NC-NPG was dominated by the dislocation nucleation at grain boundaries, the $\Delta\sigma/\sigma^{\rm CLN}$ of NC-NPG would be smaller than that of CG-NPG, which contradicts our observation. Figure 4(c) shows the traces of surface dislocation nucleation in deformed NC-NPG, which has also been observed in CG-NPGs. These results support the scenario that dislocation nucleations at STJs and surfaces are competing mechanisms dominating the plastic deformation of sub-100 nm scale crystals.

Although grain boundaries are buried in bulk and insensitive to electrochemical modification, a specific type of grain-boundary-mediated deformation, i.e., grain boundary sliding, could also create new surface and may be

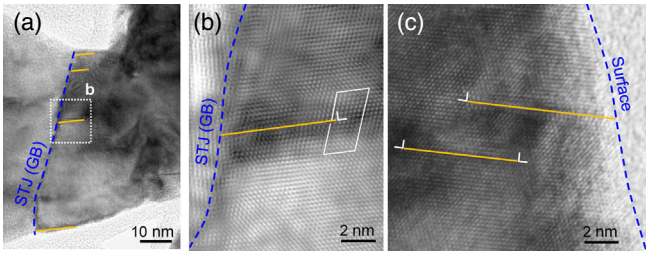

FIG. 4. Traces of dislocation nucleation in NC-NPG. HR-TEM images showing stacking faults (indicated by yellow lines) bounded by (a-b) a grain boundary or surface triple junction and (c) the surface. The other ends of stacking faults terminate in Shockley partial dislocations. Ligament size is approximately 45 nm. Compression strain is approximately 0.10. Most of these stacking faults were eventually removed by trailing partials to form full dislocations, as frequently seen in the deformed structures of CG- and NC-NPGs ($L = 45$ nm) with different surface states (Figs. S9–S12 [17]).

affected by electrochemical modifications, particularly in nanoscale ligaments. However, TEM examinations did not provide conclusive evidence for grain boundary sliding in the deformation of NC-NPGs (see Fig. 4 and Figs. S11–S12). This indicates insignificant (if not zero) contribution of grain boundary sliding to the plastic deformation of NC-NPGs and thus the STJ effect observed in this study. Nevertheless, grain boundary sliding has been observed in other nanoscale metals under certain loading conditions [41]. Whether and how grain boundary sliding contributes to STJ effect deserve more in-depth study in future, particularly in sub-10 nm scale polycrystalline solids.

This study reveals that STJs are not simply geometrical intersection lines shared by surfaces and grain boundaries. Instead, STJs can contribute to the strength of nanoscale materials. The STJ effect is different from and even prevail over surface and grain-boundary effects when sample and grain sizes enter sub-100 nm region. We anticipate that STJ modification or STJ engineering, and triple-junction engineering in a more general sense, will be explored to tailor the mechanical properties of nanomaterials for many applications. Our findings might also shed new light on the understanding of STJ-initiated failures, such as the stress corrosion cracking [42,43] of engineering alloys.

Supported by the National Natural Science Foundation of China (Grant No. 51971218) and the National Key R&D Program of China (Grant No. 2017YFA0204401). We thank Prof. Ke Lu for fruitful discussions and a critical reading of the paper, and Prof. Huiling Duan for valuable comments.

*Corresponding author.
hjjin@imr.ac.cn

[1] A. H. King, Triple lines in materials science and engineering, Scr. Mater. **62**, 889 (2010).
[2] H. B. Huang and F. Spaepen, Tensile testing of free-standing Cu, Ag and Al thin films and Ag/Cu multilayers, Acta Mater. **48**, 3261 (2000).
[3] J. R. Greer and J. T. M. De Hosson, Plasticity in small-sized metallic systems: Intrinsic versus extrinsic size effect, Prog. Mater. Sci. **56**, 654 (2011).
[4] T. Zhu and J. Li, Ultra-strength materials, Prog. Mater. Sci. **55**, 710 (2010).
[5] C. Deng and F. Sansoz, Near-ideal strength in gold nanowires achieved through microstructural design, ACS Nano **3**, 3001 (2009).
[6] Y. Kim, S. Lee, J. B. Jeon, Y. J. Kim, B. J. Lee, S. H. Oh, and S. M. Han, Effect of a high angle grain boundary on deformation behavior of Al nanopillars, Scr. Mater. **107**, 5 (2015).
[7] C. V. Thompson, Grain-growth in thin films, Annu. Rev. Mater. Sci. **20**, 245 (1990).
[8] B. Zhao, G. Gottstein, and L. S. Shvindlerman, Triple junction effects in solids, Acta Mater. **59**, 3510 (2011).
[9] K. C. Chen, W. W. Wu, C. N. Liao, L. J. Chen, and K. N. Tu, Observation of atomic diffusion at twin-modified grain boundaries in copper, Science **321**, 1066 (2008).
[10] X. P. Zhang, J. Han, J. J. Plombon, A. P. Sutton, D. J. Srolovitz, and J.J . Boland, Nanocrystalline copper films are never flat, Science **357**, 397 (2017).
[11] R. G. Mariano, K. McKelvey, H. S. White, and M. W. Kanan, Selective increase in CO_2 electroreduction activity at grain-boundary surface terminations, Science **358**, 1187 (2017).
[12] S. Kobayashi, S. Tsurekawa, and T. Watanabe, Grain boundary hardening and triple junction hardening in polycrystalline molybdenum, Acta Mater. **53**, 1051 (2005).
[13] L. J. Gibson and M. F. Ashby, *Cellular Solids: Structure and Properties*, 2 ed. (Cambridge University Press, Cambridge, Engalnd, 1997).
[14] G. Palumbo, U. Erb, and K. T. Aust, Triple line disclination effects on the mechanical behavior of materials, Scr. Metall. Mater. **24**, 2347 (1990).
[15] J. Erlebacher, M. J. Aziz, A. Karma, N. Dimitrov, and K. Sieradzki, Evolution of nanoporosity in dealloying, Nature (London) **410**, 450 (2001).
[16] J. Weissmueller, R. C. Newman, H.-J. Jin, A. M. Hodge, and J. W. Kysar, Nanoporous metals by alloy corrosion: Formation and mechanical properties, MRS Bull. **34**, 577 (2009).
[17] See Supplemental Material at http://link.aps.org/supplemental/10.1103/PhysRevLett.126.235501 for experimental details and Figs. S1–S12, which includes Refs. [18–25].
[18] H. J. Jin and J. Weissmuller, A material with electrically tunable strength and flow stress, Science **332**, 1179 (2011).
[19] L. Z. Liu, X. L. Ye, and H. J. Jin, Interpreting anomalous low-strength and low-stiffness of nanoporous gold: Quantification of network connectivity, Acta Mater. **118**, 77 (2016).
[20] L. Z. Liu and H. J. Jin, Scaling equation for the elastic modulus of nanoporous gold with "fixed" network connectivity, Appl. Phys. Lett. **110**, 211902 (2017).
[21] Y. H. Xiang, L. Z. Liu, J. C. Shao, and H. J. Jin, A universal scaling relationship between the strength and Young's modulus of dealloyed porous $Fe_{0.80}Cr_{0.20}$, Acta Mater. **186**, 105 (2020).
[22] K. S. Ng and A. H. W. Ngan, Deformation of micron-sized aluminium bi-crystal pillars, Philos. Mag. **89**, 3013 (2009).
[23] A. Kunz, S. Pathak, and J. R. Greer, Size effects in Al nanopillars: Single crystalline vs. bicrystalline, Acta Mater. **59**, 4416 (2011).
[24] P. Liu, X. Wei, S. X. Song, L. H. Wang, A. Hirata, T. Fujita, X. D. Han, Z. Zhang, and M. W. Chen, Time-resolved atomic-scale observations of deformation and fracture of nanoporous gold under tension, Acta Mater. **165**, 99 (2019).
[25] P. Liu, L. H. Wang, Y. H. Yue, S. X. Song, X. D. Wang, K. M. Reddy, X. Z. Liao, Z. Zhang, M. W. Chen, and X. D. Han, Room-temperature superplasticity in Au nanowires and their atomistic mechanisms, Nanoscale **11**, 8727 (2019).
[26] Z. L. Wang, S. C. Ning, P. Liu, Y. Ding, A. Hirata, T. Fujita, and M. W. Chen, Tuning surface structure of 3D nanoporous gold by surfactant-free electrochemical potential cycling, Adv. Mater. **29**, 7 (2017).
[27] K. Sieradzki, Potential solutions for creating responsive materials, Science **332**, 1158 (2011).

[28] P. Wu, X. L. Ye, L. Z. Liu, and H. J. Jin, Monolayer oxide enhanced flow stress in nanoporous gold: The size dependence, Mater. Res. Lett. **6**, 508 (2018).
[29] N. Mameka, J. Markmann, and J. Weissmüller, On the impact of capillarity for strength at the nanoscale, Nat. Commun. **8**, 1976 (2017).
[30] S. Yin, G. M. Cheng, T. H. Chang, G. Richter, Y. Zhu, and H. J. Gao, Hydrogen embrittlement in metallic nanowires, Nat. Commun. **10**, 9 (2019).
[31] M. T. Kiani, R. P. Patil, and X. W. D. Gu, Dislocation surface nucleation in surfactant-passivated metallic nanocubes, MRS Commun. **9**, 1029 (2019).
[32] H. J. Jin, J. Weissmuller, and D. Farkas, Mechanical response of nanoporous metals: A story of size, surface stress, and severed struts, MRS Bull. **43**, 35 (2018).
[33] K. R. Mangipudi, E. Epler, and C. A. Volkert, Topology-dependent scaling laws for the stiffness and strength of nanoporous gold, Acta Mater. **119**, 115 (2016).
[34] N. Mameka, K. Wang, J. Markmann, E. T. Lilleodden, and J. Weissmueller, Nanoporous gold-testing macro-scale samples to probe small-scale mechanical behavior, Mater. Res. Lett. **4**, 27 (2016).
[35] A. T. Jennings, J. Li, and J. R. Greer, Emergence of strain-rate sensitivity in Cu nanopillars: Transition from dislocation multiplication to dislocation nucleation, Acta Mater. **59**, 5627 (2011).
[36] T. Zhu, J. Li, A. Samanta, A. Leach, and K. Gall, Temperature and Strain-Rate Dependence of Surface Dislocation Nucleation, Phys. Rev. Lett. **100**, 025502 (2008).
[37] W. B. Liu, Y. Liu, Y. Y. Cheng, L. R. Chen, L. Yu, X. Yi, and H. L. Duan, Unified Model for Size-Dependent to Size-Independent Transition in Yield Strength of Crystalline Metallic Materials, Phys. Rev. Lett. **124**, 235501 (2020).
[38] J. Shin, L. Y. Chen, U. T. Sanli, G. Richter, S. Labat, M. I. Richard, M. I. Richard, O. Thomas, and D. S. Gianola, Controlling dislocation nucleation-mediated plasticity in nanostructures via surface modification, Acta Mater. **166**, 572 (2019).
[39] J. Li, Diffusive origins, Nat. Mater. **14**, 656 (2015).
[40] L. Y. Chen, M. R. He, J. Shin, G. Richter, and D. S. Gianola, Measuring surface dislocation nucleation in defect-scarce nanostructures, Nat. Mater. **14**, 707 (2015).
[41] X. W. Gu, C. N. Loynachan, Z. Wu, Y.-W. Zhang, D. J. Srolovitz, and J. R. Greer, Size-dependent deformation of nanocrystalline Pt nanopillars, Nano Lett. **12**, 6385 (2012).
[42] N. Badwe, X. Chen, D. K. Schreiber, M. J. Olszta, N. R. Overman, E. K. Karasz, A. Y. Tse, S. M. Bruemmer, and K. Sieradzki, Decoupling the role of stress and corrosion in the intergranular cracking of noble-metal alloys, Nat. Mater. **17**, 887 (2018).
[43] S. F. Sun, X. Y. Chen, N. Badwe, and K. Sieradzki, Potential-dependent dynamic fracture of nanoporous gold, Nat. Mater. **14**, 894 (2015).